Eur. Phys. J. A **8**, 115–124 (2000)

THE EUROPEAN PHYSICAL JOURNAL A

Effect of shell structure on energy dissipation in heavy-ion collisions

R.V. Jolos[1], A.K. Nasirov[1,2,a], G.G. Adamian[2,3], and A.I. Muminov[2]

[1] Joint Institute for Nuclear Research, 141980, Dubna, Russia
[2] Heavy Ion Physics Department, Institute of Nuclear Physics, 702132 Ulugbek, Tashkent, Uzbekistan
[3] Institut für Theoretische Physik der Justus-Liebig-Universität, D-35392 Giessen, Germany

Received: 27 July 1999 / Revised version: 2 February 2000
Communicated by P. Schuck

Abstract. The effect of shell structure on the distribution of the excitation energy between fragments of the deep inelastic collisions is analysed in the microscopic approach. It is shown that the density of the single-particle levels of the proton and neutron subsystems near the Fermi surface determines the ratio between the excitation energies of fragments at the initial stage of the collision. It is shown also that the shell structure strongly influences the correlations between the width of the charge distributions and the total kinetic energy losses. Calculations are performed for the ^{40,48}Ca+^{248}Cm reactions. The results obtained suggest a possible interpretation for the observed concentration of the excitation energy in the light fragment in deep inelastic collisions for a wide range of the total kinetic energy losses.

PACS. 25.70.Hi Transfer reactions – 25.70.Lm Strongly damped collisions

1 Introduction

Dissipation of a large amount of the kinetic energy in deep inelastic heavy-ion collisions (DIC) is a fundamental time-dependent process [1,2] that has attracted theoretical interest since the discovery of this class of reactions. At an earlier stage of investigations it was assumed that the excitation energy is distributed between reaction partners in proportion to their masses. However, after a series of experiments, it became clear that a large part of the excitation energy is concentrated in the light fragments for a wide range of total kinetic energy losses (TKEL). Various models have been proposed to explain this phenomenon, taking into account a coupling of the relative motion to the intrinsic degrees of freedom. The simple macroscopic models with phenomenological friction forces cannot be used to treat this problem. In microscopic models, friction forces are derived considering a coupling of the relative motion to the specific intrinsic degrees of freedom. However, not all of these models can consider a division of the excitation energy between the reaction partners.

To microscopic models, which can make predictions for the excitation energy partitioning between the reaction partners, belong the model developed in [3]. In this model, all transport phenomena are assumed to be mediated by the exchange of independent nucleons between interacting nuclei. Sufficient amounts of the kinetic energy is dissipated when large numbers of nucleons are transferred in alternating directions. Usually, in deep inelastic heavy-ion collisions, a shift of the centroid of the mass distributions is small in comparison with the width. Therefore, it is expected that both nuclei receive, on the average, comparable amounts of excitation energy. In the model [3], which is based on the Fermi-gas model for the intrinsic motion, the kinetic energy losses are explained by the fact that the intrinsic momentum of a transferred nucleon is summed with the momentum of the relative motion. As a result, this momentum can be larger than the Fermi momentum $P_{\rm F}$, thus producing the excitation of a donor nucleus.

For relative velocities of the interacting nuclei at which the adiabatic approximation loses its accuracy, the model developed in [4,5] suggests that particle-hole states are excited in the two interacting nuclei as a result of diabatic transitions between the single-particle levels of a time-dependent one-body potential. Thus, in this model, a description of the dissipative processes is strongly based on the single-particle level schemes in the two-center potential well of a dinuclear system. Detailed calculations based on this model for the ^{139}La+^{109}Ag reaction [6] have shown that the excitation energy per nucleon ϵ^* is smaller for the heavier reaction partner. At the same time, it is known from the calculations of inelastic processes in nucleus-nucleus collisions that appreciable energy dissipation takes place even before the first crossing of the single-particle levels near the Fermi surface [7]. Therefore, it is necessary to look for other possibilities to explain an ob-

[a] Bogoliubov Laboratory of Theoretical Physics JINR, 141980, Dubna, Russia.
e-mail: nasirov@thsun1.jinr.ru

served partition of the excitation energy between reaction partners.

The important aspect of the description of a nucleon transfer and a kinetic energy dissipation is connected with an influence of the peculiarities of the shell structure of the interacting nuclei on the correlations between the kinetic energy loss and the width of the fragment charge distribution. Indeed, it was demonstrated in [1,8–11] by analysing the experimental data for different reactions that these correlations are sensitive to the projectile-target combination. So, it is interesting also to investigate the effect of the shell structure near the Fermi surface on the sharing of the excitation energy between fragments of binary reactions. This is the aim of the present paper.

In fact, we will investigate the influence of the single-particle level density near the Fermi surface on these characteristics. The calculations are performed with the experimentally determined single-particle scheme of Ca isotopes and with the single-particle scheme in which the level density is doubled artificially. In both cases the proton and neutron separation energies remain constant at the beginning of interaction. However, a number of the single-particle states taken into account is increased accordingly to the scaling of the single-particle scheme. In [12–15], we developed a microscopic approach to describe the loss of the total kinetic energy and its partitioning between the reaction partners in DIC. The particle-hole excitation and the nucleon exchange are responsible for this dissipation mechanism. Using this model, we have successfully described different characteristics of deep inelastic reactions, such as the centroid positions and the width of the mass and charge distributions as functions of the excitation energy and partition of the excitation energy between the reaction product [12,15].

Comparing our model to the model [3], we should mention that in principle the effect of the addition of relative and intrinsic nucleon momenta can be taken into account in the framework of our approach. In order to do this, it is necessary to transform the Hamiltonian into an intrinsic frame. Then, the additional terms depending on the velocity of the relative motion will appear in the Hamiltonian. These new terms will contribute to the matrix elements of the single nucleon transfer and, therefore, will influence the kinetic energy dissipation process. However, this effect is not included in the present calculations.

2 Model

It is convenient to start with the total Hamiltonian of a dinuclear system written in the form

$$\hat{H} = \hat{H}_{\rm rel}(\mathbf{R};\mathbf{P}) + \hat{H}_{in}(\xi) + \delta\hat{V}(\mathbf{R},\xi), \tag{1}$$

where the Hamiltonian of a relative motion,

$$\hat{H}_{\rm rel}(\mathbf{R};\mathbf{P}) = \frac{\hat{\mathbf{P}}^2}{2\mu} + \hat{U}(\hat{\mathbf{R}}), \tag{2}$$

consists of the kinetic energy operator and the nucleus-nucleus interaction potential $\hat{U}(\hat{\mathbf{R}})$. Here, $\hat{\mathbf{R}}$ is the relative distance between the centers of mass of the fragments, $\hat{\mathbf{P}}$ is the conjugate momentum, and μ is the reduced mass of the system; ξ is a set of relevant intrinsic variables. The last two terms in (1) describe the internal motion of nuclei and the coupling between the relative and internal motions (for details, see [12,13]). It is clear that the coupling term leads to a dissipation of the kinetic energy into the energy of the internal nucleon motion and to an increase of the attractive part of nucleus-nucleus potential [14]. Our further consideration will be concentrated on this term.

Let us take a sum of the last two terms in (1) as a single-particle Hamiltonian of a dinuclear system $\hat{\mathcal{H}}$ plus a residual interaction,

$$\hat{H}_{\rm in}(\xi) + \delta\hat{V}(\mathbf{R},\xi) = \hat{\mathcal{H}}(\mathbf{R},\xi) + h_{\rm residual},$$
$$\hat{\mathcal{H}}(\mathbf{R}) = \sum_{i=1}^{A}\left(\frac{-\hbar^2}{2m}\Delta_i + \hat{V}_P(\mathbf{r}_i - \mathbf{R}) + \hat{V}_T(\mathbf{r}_i)\right), \tag{3}$$

where m is the nucleon mass and $A = A_P + A_T$ is the total number of nucleons in the system.

Then, in the second quantization representation, the Hamiltonian $\hat{\mathcal{H}}(\mathbf{R},\xi)$ can be written as

$$\hat{\mathcal{H}}(\mathbf{R},\xi) = \sum_P \varepsilon_P \mathrm{a}_P^\dagger \mathrm{a}_P + \sum_T \varepsilon_T \mathrm{a}_T^\dagger \mathrm{a}_T + \sum_{i,i'} V_{ii'}(\mathbf{R})\mathrm{a}_i^\dagger \mathrm{a}_{i'}, \tag{4}$$

where

$$\sum_{i,i'} V_{ii'}(\mathbf{R})\mathrm{a}_i^\dagger \mathrm{a}_{i'} = \sum_{T,P} \mathrm{g}_{PT}(\mathbf{R})(\mathrm{a}_P^\dagger \mathrm{a}_T + \mathrm{H.c.}) + \sum_{P,P'} \Lambda^{(T)}_{PP'}(\mathbf{R})\mathrm{a}_P^\dagger \mathrm{a}_{P'} + \sum_{T,T'} \Lambda^{(P)}_{TT'}(\mathbf{R})\mathrm{a}_T^\dagger \mathrm{a}_{T'}\,. \tag{5}$$

Here $P \equiv (n_P, j_P, l_P, m_P)$ and $T \equiv (n_T, j_T, l_T, m_T)$ are the sets of quantum numbers characterizing the single-particle states. The single-particle basis is constructed basing on the single-particle states of the noninteracting nuclei—the projectile ion $|P\rangle$ and the target nucleus $|T\rangle$. Since $|P\rangle$ and $|T\rangle$ being the eigenstates of different Hamiltonians are not orthogonal, at first, we orthogonalized them approximately

$$|\tilde{P}\rangle = |P\rangle - \frac{1}{2}\sum_T |T\rangle\langle T|P\rangle, \tag{6}$$

$$|\tilde{T}\rangle = |T\rangle - \frac{1}{2}\sum_P |P\rangle\langle P|T\rangle. \tag{7}$$

For this basis set, the orthogonality condition is satisfied up to terms linear in $\langle P|T\rangle$. Then

$$\Lambda^{(T)}_{PP'}(\mathbf{R}) = \langle P|V_T(\mathbf{r})|P'\rangle, \tag{8}$$

$$\Lambda^{(P)}_{TT'}(\mathbf{R}) = \langle T|V_P(\mathbf{r}-\mathbf{R})|T'\rangle, \tag{9}$$

$$g_{PT}(\mathbf{R}(t)) = \frac{1}{2}\langle P|V_P(\mathbf{r}-\mathbf{R}) + V_T(\mathbf{r})|T\rangle. \tag{10}$$

The nondiagonal matrix elements $\Lambda^{(T)}_{PP'}$ ($\Lambda^{(P)}_{TT'}$) generate the particle-hole excitations in the projectile (target) nucleus. The matrix elements g_{PT} are responsible for the nucleon exchange between reaction partners. These matrix elements were calculated using the method proposed in [16,17]. The coupling between the intrinsic nuclear degrees of freedom and the collective variable **R** is introduced by the **R** dependence of the sum of the single-particle potentials in (3). During reactions the energies and the wave functions of the single-particle states of the interactive nuclei are disturbed by the mean field of the reaction partner nucleus. However, because of the small overlap of the interactive nuclei in DIC ($V_{\rm overlap}/(V_P + V_T) \approx 0.06$) this effect can be taken into account in the perturbation calculations. This assumption is confirmed by the calculations of the single-particle basis in the strongly deformed nuclei, when the radius of a neck connecting two clusters forming compound nucleus, is small. It was shown in [18,19] that in this case the single-particle scheme of the compound nucleus is a superposition of the single-particle schemes of the isolated clusters, with a good accuracy.

Thus,

$$|\tilde{P}\rangle \longrightarrow |\tilde{P}\rangle + \sum_{P'} \frac{\Lambda^{(T)}_{PP'}(R)}{\varepsilon_P - \varepsilon_{P'}} |\tilde{P}'\rangle, \tag{11}$$

$$|\tilde{T}\rangle \longrightarrow |\tilde{T}\rangle + \sum_{T'} \frac{\Lambda^{(P)}_{TT'}(R)}{\varepsilon_T - \varepsilon_{T'}} |\tilde{T}'\rangle \tag{12}$$

and the renormalized single-particle energies are

$$\tilde{\varepsilon}_P(\mathbf{R}) = \varepsilon_P + \langle P|V_T(\mathbf{r})|P\rangle, \tag{13}$$

$$\tilde{\varepsilon}_T(\mathbf{R}) = \varepsilon_T + \langle T|V_P(\mathbf{r}-\mathbf{R})|T\rangle. \tag{14}$$

In (13) and (14) $\epsilon_{P(T)}$ are the single-particle energies of the nonperturbed states of the projectile (target) nucleus. As a result the matrix elements $\Lambda^{(T)}_{PP'}$, ($\Lambda^{(P)}_{TT'}$) and g_{PT} are renormalized also

$$V_{ii'}\ (R) \longrightarrow V_{ii'}(R) + \sum_k V_{ik}(R)V_{ki'}(R)\left(\frac{1}{\varepsilon_i - \varepsilon_k} + \frac{1}{\varepsilon'_i - \varepsilon_k}\right). \tag{15}$$

Numerically, the contribution of the correction terms are small, however, they are taken into account in the calculations below. Note also the effect of a nucleon exchange on the single-particle energies used in the calculations. Of course when atomic and mass numbers of the interacting nuclei change during a collision, their mean fields change also. However, since a centroid shift of the charge or mass distribution is usually small in DIC, we neglect this effect in the calculations below. Of course the evolution of the occupation numbers of the single-particle states produced by excitations of nuclei or by nucleon exchange is a very important effect and is taken into account.

Since explicit allowance for the residual interaction requires extensive calculations, it is customary to take the two-particle collision integral into account in a linearized form (τ-approximation) [12,13]:

$$i\hbar\frac{\partial\hat{\tilde{n}}(t)}{\partial t} = [\hat{\mathcal{H}}(\mathbf{R}), \hat{\tilde{n}}(t)] - \frac{i\hbar}{\tau}[\hat{\tilde{n}}(t) - \hat{\tilde{n}}^{\rm eq}(\mathbf{R})], \tag{16}$$

where $\tilde{n}^{\rm eq}(R)$ is a local quasi-equilibrium distribution, *i.e.*, a Fermi distribution with the temperature T corresponding to the excitation energy at the internuclear distance **R**:

$$\tilde{n}^{\rm eq}_i(R) = \left[1 + \exp\Big(\frac{\tilde{\varepsilon}_i(R) - \lambda(R)}{T}(R)\Big)\right]^{-1}. \tag{17}$$

In (17) λ is the chemical potential for the considered neutron or proton subsystems. The chemical potential for neutrons $\lambda^N_{P(T)}$ and protons $\lambda^Z_{P(T)}$ of the projectile like "P" and target like "T" nuclei are calculated using at each time step the conditions

$$N_P(t) = \sum_i (2j_i + 1)\tilde{n}^{\rm eq}_i(t),$$

where j_i is an angular momentum of the single-particle state i. The number of particles at the moment t, $N_P(t)$, is determined by the sum of the initial number of particles and a shift of the centroid of the particle distribution to the moment t. The effective temperatures of the interacting nuclei were calculated by the expression

$$T_{P(T)}(t) = 3.46\ \sqrt{E^*_{P(T)}(t)/A_{P(T)}(t)} \tag{18}$$

at the current time t. The excitation energies $E^*_{P(T)}(t)$ are determined below by (28). In nuclear matter calculations the relaxation time approximation was used in [20–22]. This way is justified, because, at the excitation energies, which are realized typically in DIC the mean free path of nucleons in nuclei is comparable to nuclear radius due to the Pauli principle. Therefore the effect of the residual two-body interaction is relatively small. Due to the small value of nuclei temperature at the beginning of the calculation, the difference between nonequilibrium $\hat{\tilde{n}}(t)$ and equilibrium $\hat{\tilde{n}}^{\rm eq}(\mathbf{R})$ occupation numbers does not exceed 0.0001 for levels near the Fermi surface. During the interaction this difference does not exceed 0.3 (see figs. 3-6). At the same time, as will be shown below in section **3** the values of τ are sufficiently large. As a consequence at each step of the calculations the ratio $(\hat{\tilde{n}}(t) - \hat{\tilde{n}}^{\rm eq}(\mathbf{R}))/\tau$ replacing the collision integral is small enough to justify an assumption. So, the system is not far from the equilibrium and the kinetic equation can be linearized.

To calculate the excitation energies of the reaction partners $E^*_P(t)$ and $E^*_T(t)$, we should know the occupation numbers of the single-particle states in both nuclei. They can be found by solving the equation for the single-particle density matrix $\tilde{n}$ in the form (16). Substituting our Hamiltonian (4) into (16), we get [12,13]

$$i\hbar\frac{\partial\tilde{n}_i}{\partial t} = \sum_k [V_{ik}(\mathbf{R})\tilde{n}_{ki} - V_{ki}(\mathbf{R})\tilde{n}_{ik}] - \frac{i\hbar}{\tau_i}[\tilde{n}_i - \tilde{n}^{\rm eq}_i], \tag{19}$$

where $\tilde{n}_i$ is a diagonal and $\tilde{n}_{ik}$ is a nondiagonal matrix element of the density matrix; $\tau = \{\tau_i\}$ is the decay time of the single-particle excitations (see Appendix A). The approximate equation for nondiagonal matrix elements takes the form

$$i\hbar\frac{\partial\tilde{n}_{ik}}{\partial t} = \hbar\left[\tilde{\omega}_{ik}(\mathbf{R}) - \frac{2i}{\tau_{ik}}\right]\tilde{n}_{ik} + V_{ki}(\mathbf{R})\left[\tilde{n}_k - \tilde{n}_i\right], \quad (20)$$

where we have used the notations $\tilde{\omega}_{ik} = \left[\tilde{\varepsilon}_i - \tilde{\varepsilon}_k\right]/\hbar$ and $\tau_{ik} = \tau_i\tau_k/(\tau_i + \tau_k)$.

Substituting the solution of eq. (20) into eq. (19), we get

$$\begin{aligned}\tilde{n}_i(\bar{t}\,) = \exp\left(\frac{t-\bar{t}}{\tau_i}\right) \times \\ \times\Bigg\{\tilde{n}_i(t) + \frac{1}{\tau_i}\int\limits_t^{\bar{t}} \mathrm{d}t'\tilde{n}_i^{\mathrm{eq}}(\mathbf{R}(t'))\exp\left(\frac{t'-t}{\tau_i}\right) \\ + \sum_k \int\limits_t^{\bar{t}} \mathrm{d}t' \int\limits_t^{t'} \mathrm{d}t''\Omega_{ik}(t',t'')\exp\left(\frac{t''-\bar{t}}{\tau_{ik}}\right) \\ \times[\tilde{n}_k(t'') - \tilde{n}_i(t'')]\Bigg\}, \end{aligned} \quad (21)$$

where

$$\begin{aligned}\Omega_{ik}(t,t') = \frac{2}{\hbar^2}\mathrm{Re}\Bigg\{V_{ik}(\mathbf{R}(t))V_{ki}(\mathbf{R}(t')) \\ \times \exp\left[i\int\limits_{t'}^{t}\mathrm{d}t''\tilde{\omega}_{ki}(\mathbf{R}(t''))\right]\Bigg\}. \end{aligned} \quad (22)$$

The formal solution of eq. (21) is found by dividing the interval $\bar{t} - t$ into small steps Δt and using the assumption $\tilde{\omega}_{ki}(R(t'')) \approx \tilde{\omega}_{ki}(R(t'))$ which is acceptable because of the smallness of the time step Δt, which is taken to be equal to $0.8 \cdot 10^{-22}$ s. Δt characterizes the time interval during which the **R**-dependent mean field of the combined dinuclear system changes so little that we can neglect the effect of this changing on the intrinsic motion. Note that an intensive dissipation of the relative kinetic energy into an intrinsic excitation energy of the interacting nuclei takes place at the values of $R(t)$ corresponding to the minimum of the nucleus-nucleus potential where the velocity of the relative motion increases after overcoming the Coulomb barrier and the friction coefficient for relative motion increases with an increase of the overlap between the mean fields of the interacting nuclei [14]. Because of proportionality of the friction forces to the velocity of the relative motion, dissipation of the kinetic energy will be more intensive when dinuclear system moves over the potential minimum. In our calculations, for the initial value of the effective temperature, we used $T(0)$=0.05 MeV. According to the expressions (13), the changes of the single-particle energies are mainly due to the diagonal matrix elements of the average potential of the partner nucleus which are functions of the relative distance $R(t)$. From (20) we derive that

$$\begin{aligned}\tilde{n}_i(t+\Delta t) = \tilde{n}_i^{\mathrm{eq}}(\mathbf{R}(t+\Delta t))\left[1 - \exp\left(\frac{-\Delta t}{\tau_i}\right)\right] \\ + n_i(t+\Delta t)\exp\left(\frac{-\Delta t}{\tau_i}\right), \end{aligned} \quad (23)$$

where

$$\begin{aligned}n_i(t+\Delta t) = \tilde{n}_i(t) \\ + \sum_k \int\limits_t^{t+\Delta t}\mathrm{d}t'\Omega_{ik}(t',t')\frac{\sin[\tilde{\omega}_{ki}(\mathbf{R}(t'))(t'-t)]}{\tilde{\omega}_{ki}(\mathbf{R}(t'))} \\ \times[\tilde{n}_k(t') - \tilde{n}_i(t')]. \end{aligned} \quad (24)$$

Note that eqs. (23) and (24) are in fact integral equations for $\tilde{n}_i(t)$.

One of our aims is to calculate the ratio of the excitation energies of the projectile-like (E_P^*) and target-like (E_T^*) fragments

$$R_{P/T} = E_P^*/E_T^*. \quad (25)$$

We defined a change of the excitation energy of the proton (P) (or neutron (N)) subsystem in each of the colliding nuclei by the following equation

$$\begin{aligned}E_P^*(t+\Delta t) = E_P^*(t) + \langle\hat{\mathcal{H}}_P(\mathbf{R},\xi) - \lambda_P\hat{N}_P\rangle_{t+\Delta t} \\ - \langle\hat{\mathcal{H}}_P(\mathbf{R},\xi) - \lambda_P\hat{N}_P\rangle_t\,. \end{aligned} \quad (26)$$

Using explicit expressions for $\hat{\mathcal{H}}_P$ and $\hat{N}_P$, as well as performing averaging, we obtain

$$\begin{aligned}E_P^*(t+\Delta t) = E_P^*(t) \\ + \sum_{i_P}\left[\Delta\varepsilon_{i_P}(t)) - \Delta\lambda_P(t)\right]\tilde{n}_{i_P}(t+\Delta t) \\ + \sum_{i_P}\left[(\tilde{\varepsilon}_{i_P}(t) - \lambda_P(t)\right]\Delta n_{i_P}(t)\,. \end{aligned} \quad (27)$$

Here $\Delta\varepsilon, \Delta n$ and $\Delta\lambda$ are the changes of the single-particle energies, the occupation numbers and the chemical potential, respectively, during time interval Δt.

Our calculations have shown that a contribution of the second term in (27) to the excitation energy is negligibly small, namely $\Delta E_P^*(t)/E_P^*(t) \leq 0.01$.

Therefore, the excitation energies of the proton $E_{P(T)}^{*(Z)}$ and neutron $E_{P(T)}^{*(N)}$ subsystems in nuclei are calculated step by step along the time scale using the equation

$$\begin{aligned}E_{P(T)}^*(t+\Delta t) = E_{P(T)}^*(t) \\ + \sum_{i_P(j_T)}\left[\tilde{\varepsilon}_{i_P(j_T)}(\mathbf{R}(t)) - \lambda_{P(T)}(\mathbf{R}(t))\right] \\ \times\left[\tilde{n}_{i_P(j_T)}(t+\Delta t) - \tilde{n}_{i_P(j_T)}(t)\right]. \end{aligned} \quad (28)$$

It should be stressed that the effect of the single-particle energy changes is taken into account in this expression,

since at every time step Δt the new values of the renormalized single-particle energies are substituted into the eq. (28) in accordance with the eq. (13).

The TKEL is defined as

$$E_{\rm loss} = E_P^* + E_T^*, \tag{29}$$

where $E_P^* = E_P^{*(Z)} + E_P^{*(N)}$ and $E_T^* = E_T^{*(Z)} + E_T^{*(N)}$. As can be seen from eqs. (21) and (22), the occupation numbers depend on an interaction matrix element $V_{ik}(\mathbf{R}(t))$, which is a short notation for $\Lambda_{PP'}^{(T)}$, $\Lambda_{TT'}^{(P)}$ describing particle-hole excitations in projectile-like and target-like nuclei, or g_{PT}, which is responsible for nucleon transfer. Thus, we can separately analyse the contribution of the two mechanisms—particle-hole excitations and the nucleon transfer—to the kinetic energy dissipation.

The variances σ_Z^2 and σ_N^2 are determined by the occupation numbers through the equation

$$\sigma_{Z(N)}^2(t) = \sum_P^{Z(N)} \tilde{n}_P(t)[1 - \tilde{n}_P(t)]. \tag{30}$$

For the well separated nuclei the nucleus-nucleus interaction potential is

$$U^{(0)} = U_{\rm C} + U_{\rm nucl} + U_{\rm rot}\ , \tag{31}$$

where $U_{\rm C}$, $U_{\rm nucl}$, and $U_{\rm rot}$ are its Coulomb, nuclear, and rotational parts, respectively. The nuclear part $U_{\rm nucl}$ was calculated by a double folding procedure of the nuclear densities and the effective nucleon-nucleon forces of Migdal [23] (for details see [14]):

$$U_{\rm nucl}(R) = \int \rho_1^{(0)}(\mathbf{r} - \mathbf{R}_1) f_{\rm eff}[\rho] \rho_2^{(0)}(\mathbf{r} - \mathbf{R}_2) \mathrm{d}^3\mathbf{r}\,, \tag{32}$$

$$f_{\rm eff}[\rho] = 300 \cdot \left(f_{\rm in} + (f_{\rm ex} - f_{\rm in}) \frac{\rho(0) - \rho(r)}{\rho(0)} \right). \tag{33}$$

Here $f_{\rm in} = 0.09$, $f_{\rm ex} = -2.59$ are the constants of the effective nucleon-nucleon interaction: $\rho = \rho_1^{(0)} + \rho_2^{(0)}$; $\mathbf{R}_i$ $(i = 1, 2)$ is the position of the center of mass of the fragment i. The nucleon densities are assumed to have a Fermi distribution. The particle-hole excitations and a nucleon exchange lead to modification of the nucleus-nucleus interaction potential

$$U^{(0)}(R) \longrightarrow U^{(0)}(R) + \delta U(R), \tag{34}$$

where the correction $\delta U(R)$ is connected with the evolution of the nuclear density. This effect was considered in [14]. The explicit expression for $\delta U(R)$ is presented in Appendix B. Our calculations have shown that the ratio $\delta U(R)/U(R)$ is equal to 0.005 in the potential well of $U(R)$.

3 Results and discussion

The well-known nonequilibrium sharing of the excitation energy between fragments of the deep inelastic collisions was reviewed in [2]. The light and heavy products of deep inelastic heavy-ion collisions are distinguished by the average energy distance between the single-particle levels near the Fermi surface: in a light fragment, this energy distance is larger than in a heavy one. For this reason, on the average, the energy of the particle-hole excitation in a light fragment is larger than in a heavy fragment. Due to this fact, it is natural to assume that the main reason for a larger excitation energy per nucleon in a light fragment is the larger energy interval between the single-particle states in the light nucleus near the Fermi surface. Below, we will check this assumption. In fact, to establish the influence of the shell structure near the Fermi surface on the nucleon transfer and the sharing of an excitation energy between the fragments of binary reactions, we will compare the results of calculations performed with the single-particle level scheme of a light nucleus that are well-established experimentally with those schemes which have an increased or decreased energy intervals compared to the experimental ones. Since the nucleon separation energy remains to be fixed, we can talk about variation of the single-particle level density near the Fermi surface. Simultaneously with a scaling of a single-particle scheme a number of the single-particle states taken into consideration is changed accordingly. In fact, where the single-particle level density of the light fragment is increased, two-three additional levels are taken into account.

As an example, consider the ^{40,48}Ca $+^{248}$Cm reactions. The calculations are performed with the experimentally determined single-particle scheme of Ca isotopes and with the single-particle scheme in which the level density is doubled artificially. The proton and neutron separation energies remain constant. The results of the calculations are shown in figs. 1a and 2a. It is seen that $R^{P/T}$ decreases with an increase of the single-particle level density near the Fermi surface of the projectile at a given TKEL ($E_{\rm loss}$). The results of calculations for other combinations of the interacting nuclei confirm this tendency.

The results of the estimation on the scale, over which the effective temperature of projectile- and target-like fragments changes, are presented by solid and dashed curves in figs. 1b and 2b for the ^{40,48}Ca + ^{248}Cm reactions, respectively. The temperature scale decreases for the projectile-like fragments (thick-dashed curve) and increases for target-like ones (thin-dashed curve) with increase of the single-particle level density near the Fermi surface of the projectile. The obtained coolness of target-like fragments in comparison with the projectile-like fragments in the reactions under discussion is confirmed by the fact that all of the observed maxima of the isotopic distributions $\langle A' \rangle_Z$ for heavy fragments are located on the neutron-rich side of the potential energy surface [24]. The authors of paper [24] concluded that the measured nuclides must have been formed cold.

Thus, we can conclude that a larger value of the excitation energy per nucleon in the light fragment is explained by its lower single-particle level density near the Fermi surface compared to a heavy fragment.

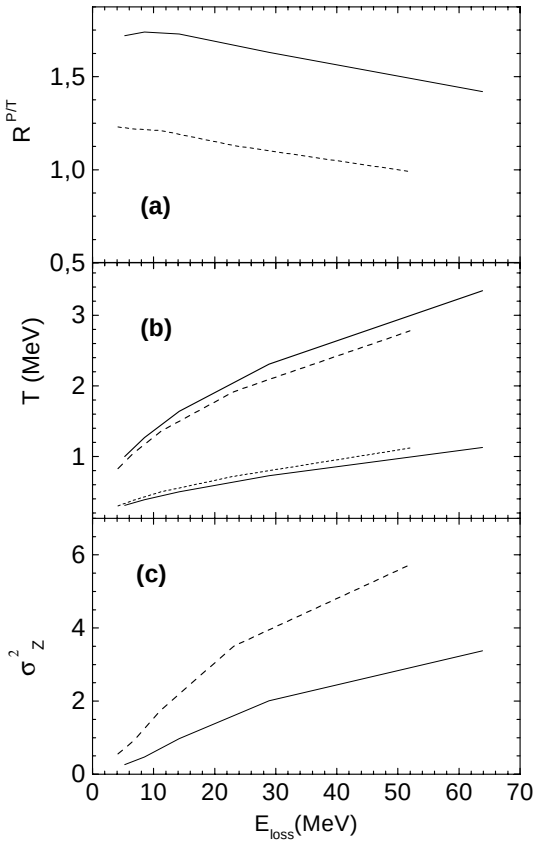

Fig. 1. The dependence of the ratio of excitation energies $R^{P/T}$ (a), the scale of temperature in projectile- (thick curves) and target-like (thin curves) fragments (b), and the charge variance σ_Z^2 (c) on $E_{\rm loss}$ for the ^{40}Ca + ^{248}Cm reaction, calculated with realistic single-particle schemes (solid curve) and with the single-particle scheme of the light fragment whose single-particle level density near the Fermi surface is doubled (dashed curve). Nucleon separation energies are the same in both cases.

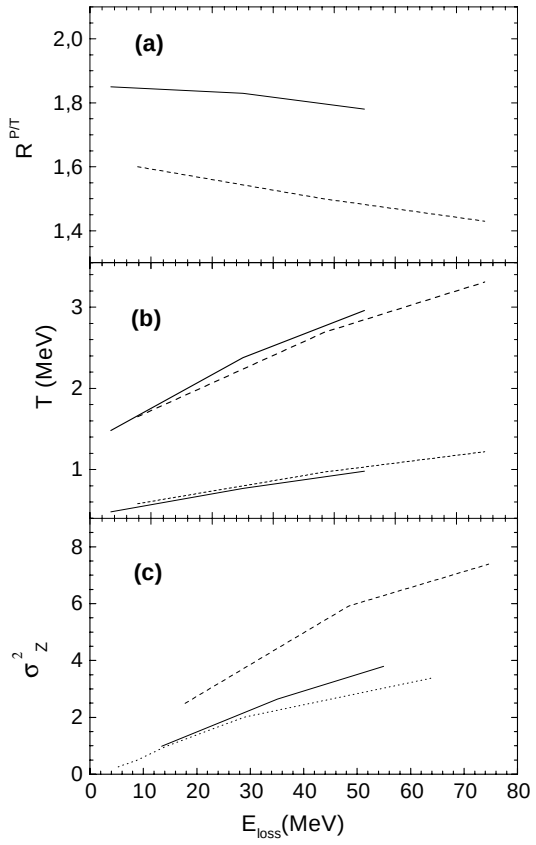

Fig. 2. The dependence of the ratio $R^{P/T}$ of excitation energies (a), the scale of temperature of projectile- (thick curves) and target-like (thin curves) fragments (b), and the charge variance σ_Z^2 (c) on $E_{\rm loss}$ for the ^{48}Ca + ^{248}Cm reaction, calculated with realistic single-particle schemes (solid curve) and with the single-particle scheme of the light fragment whose single-particle level density near the Fermi surface is doubled (dashed curve). Nucleon separation energies are the same in both cases. For comparison the charge variance σ_Z^2 on $E_{\rm loss}$ for the ^{40}Ca + ^{248}Cm reaction, calculated with realistic single-particle schemes (dotted curve), is presented.

In figs. 1c and 2c, we show the results of calculations of the charge variance σ_Z^2 as a function of the TKEL performed with different single-particle schemes for a light fragment. It is seen that σ_Z^2 increases more rapidly with an excitation energy increase if a single-particle level density at the Fermi surface of the projectile-like fragment (PLF) takes a larger value. This result is in correspondence with the experimentally observed influence of the shell structure on the correlation between the charge variance and TKEL [9,11]. It was observed that TKEL increase more rapidly with σ_Z^2 in the ^{208}Pb (7.6 MeV/A) + ^{208}Pb reaction than in the ^{208}Pb (7.5 MeV/A) + ^{238}U and ^{238}U (7.4 MeV/A) + ^{238}U reactions. In other words, at the same TKEL, σ_Z^2 is larger in reactions with ^{238}U than with ^{208}Pb. The single-particle level density near the Fermi surface in ^{238}U is also larger than in ^{208}Pb.

Now consider the influence of the scaling of a level density on the occupation numbers of the single-particle states in the interacting nuclei. In figs. 3–6, we show the occupation numbers of neutron and proton single-particle states calculated with the experimentally established (figs. 3a-6a) and compressed (figs. 3b-6b) single-particle schemes of Ca while the single-particle scheme of ^{248}Cm (figs. 3c-6c) was not changed. Notice that in the case of the compressed (figs. 3b-6b) single-particle schemes of Ca the number of the bound states increases due to the fact that the quasi-bound states become bound after scaling because of the constancy of the nucleon separation energies. It is clearly seen that with an increase of the single-particle level density near the Fermi surface, the transitional region from the occupied to the unoccupied states becomes narrower. This means that the effective temperature characterizing the single-particle occupation numbers in PLF is smaller

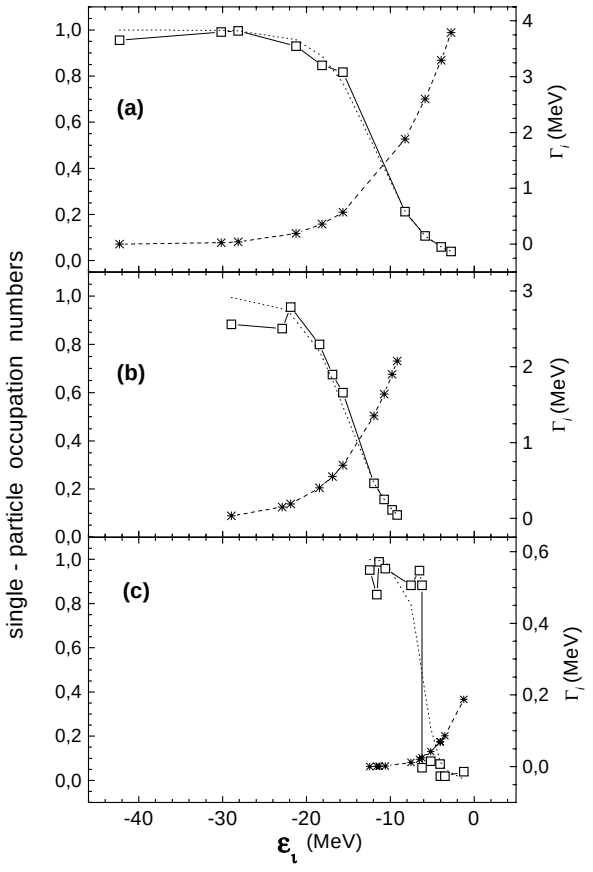

Fig. 3. The calculated dynamical (solid curve with squares) occupation numbers as functions of the neutron single-particle energies in the light fragment for the ^{40}Ca+^{248}Cm deep inelastic collision. The results are obtained with the realistic (a) and compressed (b) the single-particle scheme of ^{40}Ca while the single-particle scheme of ^{248}Cm (c) was not changed. Approximate description of the occupation numbers by the Fermi distribution function with temperature is given by the dotted curve. For these quantities, the left ordinate axis is used. The width of the single-particle levels (Γ_i) are shown by dashed curves with stars (right ordinate axis).

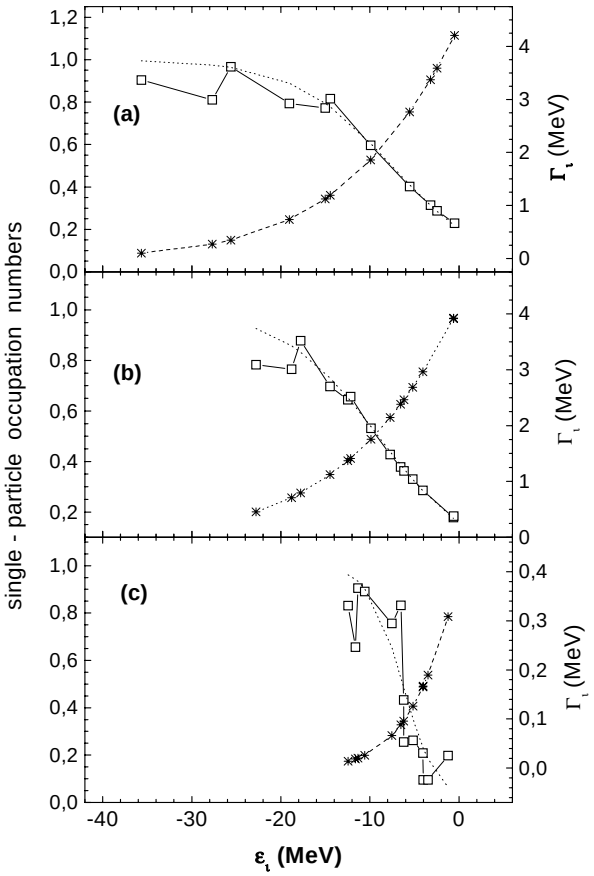

Fig. 4. The same as in fig. 3, but for the neutron subsystem in the ^{48}Ca +^{248}Cm reaction.

for the larger level density if the reaction conditions, including the bombarding energy, are the same. For clarity, we have shown also the results of the approximate description of the calculated occupation numbers by the smooth Fermi distribution function with temperature fixed to get a better fit (figs. 3a-6a).

A decrease in the effective temperature characterizing the nucleon occupation numbers in the reaction products with an increase of the single-particle level density near the Fermi surface is just in correspondence with the results demonstrated in figs. 1, 2. The calculations are done for two projectile-target combinations, ^{40,48}Ca + ^{248}Cm. In these cases, the projectiles differ by the positions of the chemical potential. Note that the lowest single-particle levels in ^{248}Cm were not included in the calculations because of the small changes of their occupation numbers. They are not presented in figs. 3c-6c. Thus, a density of the single-particle levels near the Fermi surface plays a crucial role in the generation of the excitation energy of nuclei.

The relaxation times of the single-particle levels τ_i used in the calculations of an evolution of the single-particle occupation numbers are calculated according to formula (A.1). Near the Fermi surface τ_i changes from $1.7{\cdot}10^{-22}$ s to $6.5{\cdot}10^{-19}$ s. The equilibration time for a Fermi-gas was estimated by Bertsch [20]

$$\tau = 2 \cdot 10^{-22}\mathrm{s\,MeV}/\epsilon^*(t), \qquad (35)$$

where $\epsilon^*(t)$ is the total excitation energy per nucleon. For the reactions under consideration τ is near 10^{-21} which is comparable with the values of τ_i obtained for levels near the Fermi surface.

The values of τ_i are related to the width of the single-particle states Γ_i by $\Gamma_i = \hbar/\tau_i$. The values of Γ_i corresponding to the excitation energies realized at the end of the reaction ($t_{\mathrm{reaction}} = 2 \cdot 10^{-21}$s) are presented in figures 3-6 by the dashed curve with stars (right axis). Thus the term $\frac{\hbar}{\tau}(\tilde{n}_i - \tilde{n}^{\mathrm{eq}_i})$ in (19) does not exceed 0.025.

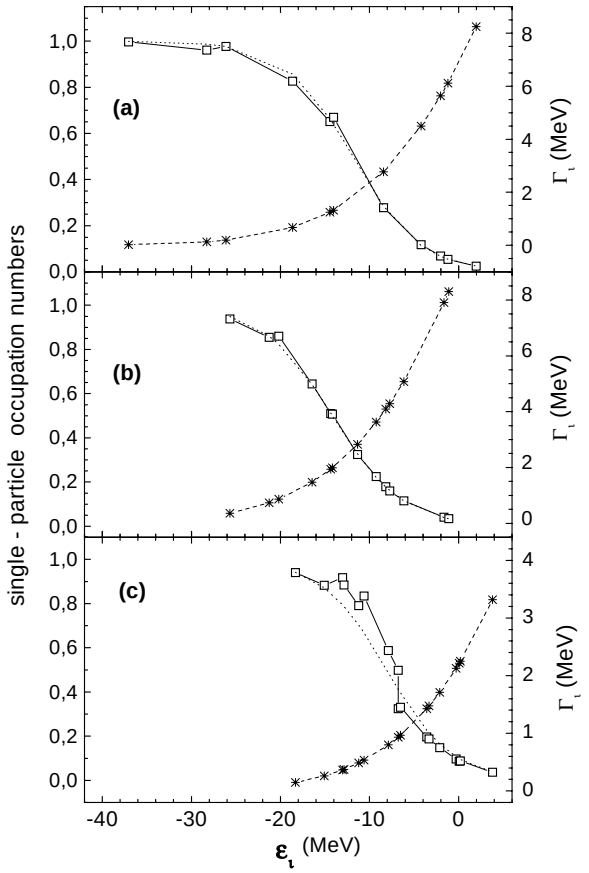

Fig. 5. The same as in fig. 3, but for the proton subsystem in the ^{48}Ca +^{248}Cm reaction.

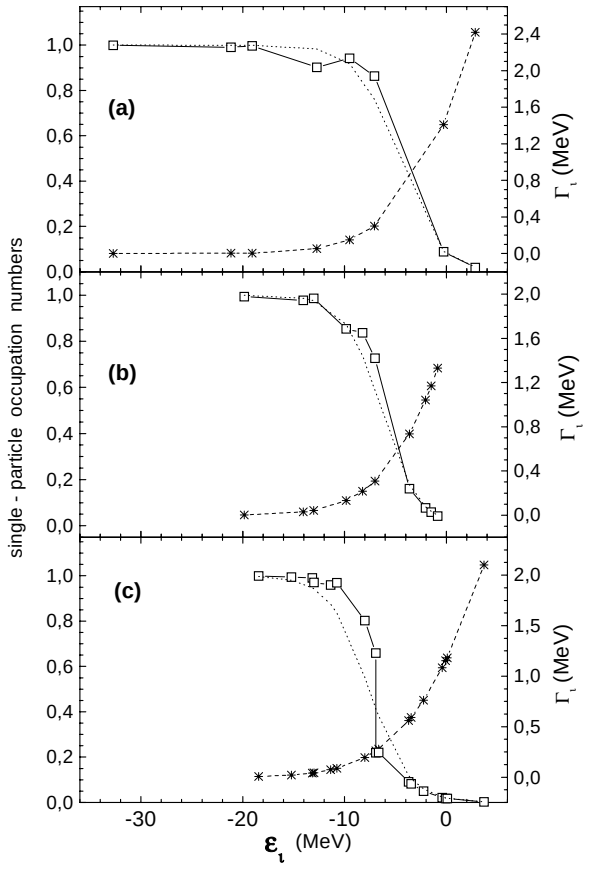

Fig. 6. The same as in fig. 3, but for the proton subsystem in the ^{40}Ca+^{248}Cm reaction.

Closing this section, consider some other effects of the shell structure. It is clear that the peculiarities of the shell structure depend on the neutron numbers. For example, the proton separation energy in ^{40}Ca and ^{48}Ca differ significantly, 8.329 MeV and 15.807 MeV, respectively. To see this effect, it is interesting to compare the values of $R^{P/T}$ presented in figs. 1a and 2a for ^{40}Ca +^{248}Cm and ^{48}Ca +^{248}Cm reactions. The additional neutrons in ^{48}Ca lead to an increase of the ratio $R^{P/T}$ for a given value of the total excitation energy. It correlates with the result obtained in [15] that neutrons get more excitation energy than protons.

Another effect of the increase of the neutron number of a projectile is seen in the correlation between the charge number variance, σ_Z^2, and TKEL (fig. 2c). The curve describing the dependence of σ_Z^2 on TKEL for reaction with ^{40}Ca is lower than the corresponding curve for ^{48}Ca + ^{248}Cm reaction at the large TKEL. This result is in qualitative agreement with the experimental data obtained for the reactions under consideration [24]. This effect can be explained by the difference in the proton separation energies of ^{40}Ca and ^{48}Ca. The proton separation energy for ^{48}Ca (S_P = 15.807 MeV) is larger than for ^{40}Ca (S_P = 8.329 MeV). It means that ^{48}Ca has more bound states of protons than ^{40}Ca. So, during deep inelastic collisions the ^{48}Ca can exchange by a larger number of protons with the target nucleus ^{248}Cm than ^{40}Ca. A similar result was observed in reactions with ^{248}Cm as a target and ^{48}Ca and ^{40}Ca as projectiles in [24] (see Fig. 10 therein) at $E_{\rm kin} = 1.1E_{\rm Coul}$.

4 Conclusion

We have investigated the influence of the single-particle level density of the PLF near the Fermi surface on the ratio of the excitation energies of the light and heavy fragments in DIC. It is shown that a two-fold increase of the single-particle level density of the PLF (the single-particle level scheme of the target-like fragment remains unchanged) decreases the ratio of the excitation energies of the light to heavy fragments by approximately 1.5 times. Since light fragments have smaller single-particle level densities near the Fermi surface than the heavy ones, we consider this result as an indication on the possible reason of the well-known experimental fact that the projectile-to-target excitation energy ratio is significantly larger than the ratio of their masses, as is expected according to thermody-

namical arguments. It is shown also that the difference in nucleon separation energies of ^{40}Ca and ^{48}Ca affects on the ratio of the excitation energies of the projectile- and target-like fragments, $R^{P/T}$, and the correlation between the charge number variance, σ_Z^2, and TKEL.

We are grateful to Prof. J. Randrup for helpful discussion which stimulated to write this paper. The authors (G.G.A., R.V.J., and A.K.N.) thank the DFG, the Russian Foundation of Basic Research (Grants No. 97-02-16030 and 99-02-04005) and the State Committee of Science and Technics of Uzbekistan (Grant No. 4/98) for the financial support.

Appendix A.

The value of τ_i is calculated using the results of the theory of quantum liquids [25] and the effective nucleon-nucleon forces from [23]:

$$\frac{1}{\tau_i^{(\alpha)}} = \frac{\sqrt{2}\pi}{32\hbar\varepsilon_{F_K}^{(\alpha)}}\left[(f_K-g)^2+\frac{1}{2}(f_K+g)^2\right] \times\left[\left(\pi T_K\right)^2+\left(\tilde{\varepsilon}_i-\lambda_K^{(\alpha)}\right)^2\right]\left[1+\exp\left(\frac{\lambda_K^{(\alpha)}-\tilde{\varepsilon}_i}{T_K}\right)\right]^{-1}, \quad \text{(A.1)}$$

where

$$T_K(t) = 3.46\sqrt{\frac{E_K^*(t)}{\langle A_K(t)\rangle}} \quad \text{(A.2)}$$

is the effective temperature determined by the amount of intrinsic excitation energy $E_K^* = E_K^{*(Z)} + E_K^{*(N)}$ and by the mass number $\langle A_K(t)\rangle$ (with $\langle A_K(t)\rangle = \langle Z_K(t)\rangle + \langle N_K(t)\rangle$). In addition, $\lambda_K^{(\alpha)}(t)$ and $E_K^{*(\alpha)}(t)$ are the chemical potential and intrinsic excitation energies for the proton ($\alpha = Z$) and neutron ($\alpha = N$) subsystems of the nucleus K ($K = 1$(projectile), 2(target)), respectively. Furthermore, the finite size of the nuclei and the available difference between the numbers of neutrons and protons need to use the following expressions for the Fermi energies [23]:

$$\varepsilon_{F_K}^{(Z)} = \varepsilon_{\rm F}\left[1-\frac{2}{3}\left(1+2f'_K\right)\frac{\langle N_K\rangle-\langle Z_K\rangle}{\langle A_K\rangle}\right], \quad \text{(A.3)}$$

$$\varepsilon_{F_K}^{(N)} = \varepsilon_{\rm F}\left[1+\frac{2}{3}\left(1+2f'_K\right)\frac{\langle N_K\rangle-\langle Z_K\rangle}{\langle A_K\rangle}\right], \quad \text{(A.4)}$$

where $\epsilon_{\rm F}$=37 MeV,

$$f_K = f_{\rm in} - \frac{2}{\langle A_K\rangle^{1/3}}(f_{\rm in}-f_{\rm ex}), \quad \text{(A.5)}$$

$$f'_K = f'_{\rm in} - \frac{2}{\langle A_K\rangle^{1/3}}(f'_{\rm in}-f'_{\rm ex}) \quad \text{(A.6)}$$

and $f_{\rm in} = 0.09$, $f'_{\rm in} = 0.42$, $f_{\rm ex} = -2.59$, $f'_{\rm ex} = 0.54$, $g = 0.7$ are the constants of the effective nucleon-nucleon interaction.

Appendix B.

Expressions for the friction coefficients

$$\gamma_R(R(t)) = \sum_{i,i'}\left|\frac{\partial V_{ii'}(R(t))}{\partial R}\right|^2 B_{ii'}^{(1)}(t), \quad \text{(B.1)}$$

$$\gamma_\theta(R(t)) = \frac{1}{R^2}\sum_{i,i'}\left|\frac{\partial V_{ii'}(R(t))}{\partial \theta}\right|^2 B_{ii'}^{(1)}(t), \quad \text{(B.2)}$$

and the dynamic contribution to the nucleus-nucleus potential

$$\delta V(R(t)) = \sum_{i,i'}\left|\frac{\partial V_{ii'}(R(t))}{\partial R}\right|^2 B_{ii'}^{(0)}(t), \quad \text{(B.3)}$$

were obtained in [14] by estimation of the evolution of the coupling term between the relative motion of nuclei and the nucleon motion inside nuclei; $B_{ii'}^{(0)}(t)$ and $B_{ii'}^{(1)}(t)$ are calculated as follows:

$$B_{ik}^{(n)}(t) = \frac{2}{\hbar}\int_0^t {\rm d}t'(t-t')^n \exp\left(\frac{t'-t}{\tau_{ik}}\right) \times \sin\left[\omega_{ik}\left(\mathbf{R}(t')\right)(t-t')\right]\left[\tilde{n}_k(t')-\tilde{n}_i(t')\right], \quad \text{(B.4)}$$

$$\hbar\omega_{ik} = \epsilon_i + \Lambda_{ii} - \epsilon_k - \Lambda_{kk}\,. \quad \text{(B.5)}$$

References

1. W.U. Schröder, J.R. Huizenga, in *Treatise on Heavy Ion Science*, edited by D.A. Bromley, Vol. 2 (Plenum, New York, 1984), p. 115.
2. J. Tõke, W.U. Schröder, Annu. Rev. Nucl. Part. **42**, 401 (1992).
3. J. Randrup, Nucl. Phys. A **307**, 319 (1978); **327**, 490 (1979).
4. S. Ayik, W. Nörenberg, Z. Phys. A **309**, 121 (1982).
5. K. Niita, W. Nörenberg, S.J. Wang, Z. Phys. A **326**, 69 (1987).
6. Z. He, P. Rozmej, J. Wu, W. Nörenberg, Nucl. Phys. A **473**, 342 (1987).
7. H.J. Krappe, Nucl. Phys. A **505**, 417 (1989).
8. M. Dakowski, P. Doll, A. Gobbi, U. Lynen, A. Olmi, G. Rudolf, H. Sann, R. Bock, in *Proceedings of the International Symposium on Continuum Spectra*, held in San Antonio, Texas, December, 1979, edited by T. Tamura, J.B. Natowitz, D.H. Youngblood, Vol. 2 (Harwood Academic Publishers CHUP, London, New York, 1980), p. 1.
9. M. Dakowski, P. Doll, A. Gobbi, G. Rudolf, H. Sann, R. Bock, U. Lynen, A. Olmi, Phys. Lett. B **90**, 379 (1980).
10. A. Gobbi, Nucl. Phys. A **354**, 337C (1981).
11. M. Dakowski, A. Gobbi, W. Nörenberg, Nucl. Phys. A **378**, 189 (1982).
12. G.G. Adamian, R.V. Jolos, A.K. Nasirov, Z. Phys. A **347**, 203 (1994).
13. G.G. Adamian, N.V. Antonenko, R.V. Jolos, A.K. Nasirov, Phys. Part. Nucl. A **25**, 583 (1994).
14. G.G. Adamian, R.V. Jolos, A.I. Muminov, A.K. Nasirov, Phys. Rev. C, **56**, 373 (1997).

15. G.G. Adamian, R.V. Jolos, A.I. Muminov, A.K. Nasirov, Phys. Rev. C **53**, 871 (1996).
16. G.G. Adamian, R.V. Jolos, A.K. Nasirov, Sov. J. Nucl. Phys. **55**, 660 (1992).
17. G.G. Adamian, N.V. Antonenko, R.V. Jolos, A.K. Nasirov, Nucl. Phys. A **551**, 321 (1993).
18. S. Aberg, Z. Phys. A **349**, 205 (1994).
19. S. Cwiok, W. Nazarewicz, J.X. Saladin, W. Plóciennik A. Johnson, Phys. Lett. B **322**, 304 (1994).
20. G.F. Bertsch, Z. Phys. A **289**, 103 (1978).
21. H.S. Kohler, Nucl. Phys. A **343**, 315 (1980); **378**, 159 (1982); **378**, 181 (1982).
22. M.M. Abu-Samreh, H.S. Kohler, Nucl. Phys. A **552**, 101 (1993).
23. A.B. Migdal, *Theory of the Finite Fermi-Systems and Properties of Atomic Nuclei* (Nauka, Moscow, 1983).
24. A. Türler *et al.*, Phys. Rev. C **46**, 1364 (1992).
25. D. Pines, P. Noziéres, *Theory of Quantum Liquids* (Benjamin, New York, 1966).